

Measurement of $3\pi^0$ photoproduction on the proton from threshold to 1.4 GeV

A. Starostin,^{1,*} I. M. Suarez,^{1,†} B. M. K. Nefkens,¹ J. Ahrens,² J. R. M. Annand,³
H. J. Arends,² K. Bantawa,⁴ P.A. Bartolome,² R. Beck,⁵ V. Bekrenev,⁶ A. Braghieri,⁷
D. Branford,⁸ W. J. Briscoe,⁹ J. Brudvik,¹ S. Cherepnaya,¹⁰ B.T. Dемисse,⁹
M. Dieterle,¹¹ E. J. Downie,^{2,3} L. V. Fil'kov,¹⁰ D. I. Glazier,⁸ R. Gregor,¹² E. Heid,²
D. Hornidge,¹³ I. Jaegle,¹¹ O. Jahn,² T. C. Jude,⁸ V. L. Kashevarov,¹⁰ I. Keshelashvili,¹¹
R. Kondratiev,¹⁴ M. Korolija,¹⁵ A. Koulbardis,⁶ S. Kruglov,⁶ B. Krusche,¹¹ V. Lisin,¹⁴
K. Livingston,³ I. J. D. MacGregor,³ D. M. Manley,⁴ M. Martinez,² J. C. McGeorge,³
E. F. McNicoll,³ D. Mekterovic,¹⁵ V. Metag,¹² A. Mushkarenkov,⁷ M. Oberle,¹¹
M. Ostrick,² P. Pedroni,⁷ A. Polonski,¹⁴ S. Prakhov,¹ J. Robinson,³ G. Rosner,³
T. Rostomyan,¹¹ S. Schumann,^{2,5} M. H. Sikora,⁸ D. Sober,¹⁶ I. Supek,¹⁵ M. Thiel,¹²
A. Thomas,² M. Unverzagt,^{2,5} D. P. Watts,⁸ D. Wertmueller,¹¹ and L. Witthauer¹¹

(Crystal Ball Collaboration at MAMI)

¹*University of California Los Angeles, Los Angeles, California 90095-1547, USA*

²*Institut für Kernphysik, University of Mainz, D-55099 Mainz, Germany*

³*SUPA, School of Physics and Astronomy, University of Glasgow, Glasgow G12 8QQ, UK*

⁴*Kent State University, Kent, Ohio 44242-0001, USA*

⁵*Helmholtz-Institut für Strahlen- und Kernphysik,
University of Bonn, D-53115 Bonn, Germany*

⁶*Petersburg Nuclear Physics Institute, Gatchina 188350, Russia*

⁷*INFN Sezione di Pavia, I-27100 Pavia, Italy*

⁸*School of Physics, University of Edinburgh, Edinburgh EH9 3JZ, UK*

⁹*The George Washington University, Washington, D.C. 20052, USA*

¹⁰*Lebedev Physical Institute, Moscow, 119991, Russia*

¹¹*Institut für Physik, University of Basel, CH-4056 Basel, Switzerland*

¹²*II Physikalisches Institut, University of Giessen, D-35392 Giessen, Germany*

¹³*Mount Allison University, Sackville, NB E4L 1E6, Canada*

¹⁴*Institute for Nuclear Research, Moscow 117312, Russia*

¹⁵*Rudjer Boskovic Institute, Zagreb 10002, Croatia*

¹⁶*The Catholic University of America, Washington, D.C. 20064, USA*

(Dated: November 14, 2018)

Abstract

The total cross section for $\gamma p \rightarrow 3\pi^0 p$ has been measured for the first time from threshold to 1.4 GeV using the tagged photon beam of the Mainz Microtron. The equipment utilized the Crystal Ball multiphoton spectrometer, the TAPS forward detector and a particle identification detector. The excitation function for $\sigma_{\text{total}}(\gamma p \rightarrow 3\pi^0 p)$ has two broad enhancements at $\sqrt{s} \approx 1.5$ GeV and 1.7 GeV. We obtained $\sigma_{\text{total}}(\gamma p \rightarrow 3\pi^0 p)/\sigma_{\text{total}}(\gamma p \rightarrow \eta p) = 0.014 \pm 0.001$ at $\sqrt{s} \approx 1.5$ GeV.

*starost@ucla.edu

†present address: Department of Physics, Texas A&M University, College Station, Texas 77843-4242, USA

I. INTRODUCTION

The spontaneous breaking of QCD chiral symmetry leads to formation of hadrons with mass. Restoration of chiral symmetry under certain conditions was theoretically predicted and has been looked for experimentally in nuclear media at normal density and in high-energy nuclear collisions. An experimental observation of mass degenerated chiral partners could be one of the signs of such restoration. Meanwhile, mass degenerated chiral multiplets are observed in the spectrum of excited baryons where pairs of N^* and Δ^* with the same angular momentum but opposite parities form parity doublets with nearly the same masses. Glozman was the first to point out that the existence of the parity doublets can be attributed to the restoration of chiral symmetry in highly excited hadronic states [1, 2]. The third resonance region consists of three pairs of N^* and two pairs of Δ^* (assuming the existence of the one-star $\Delta(1750)_{\frac{1}{2}}^{1+}$), which can be qualified as parity doublets, therefore the mass region around $\sqrt{s} \sim 1700$ MeV is particularly important for an experimental investigation of baryonic chiral multiplets. Decoupling of the N^* sextet that consists of $N(1650)_{\frac{1}{2}}^{1-}$, $N(1675)_{\frac{5}{2}}^{-}$, $N(1680)_{\frac{5}{2}}^{+}$, $N(1700)_{\frac{3}{2}}^{-}$, $N(1710)_{\frac{1}{2}}^{1+}$ and $N(1720)_{\frac{3}{2}}^{+}$, and the four Δ^* states ($\Delta(1600)_{\frac{3}{2}}^{+}$, $\Delta(1620)_{\frac{1}{2}}^{-}$, $\Delta(1750)_{\frac{1}{2}}^{1+}$ and $\Delta(1700)_{\frac{3}{2}}^{-}$) is however a challenging experimental task. These states are broad and overlapping. In fact, two of the six N^* , namely $N(1700)_{\frac{3}{2}}^{-}$ and $N(1710)_{\frac{1}{2}}^{1+}$, are not seen in the recent SAID partial-wave analysis (PWA) [3]. As the coupling of N^* and Δ^* to πN decreases with the increase of the incident energy, new information on decay modes other than $N^* \rightarrow \pi N$ is needed to determine the properties of the states. We have addressed this issue previously, publishing new high precision $\gamma p \rightarrow \eta p$ data [4]. In this paper we present the first measurement of the $\gamma p \rightarrow 3\pi^0 p$ reaction, which has been made at the Mainz Microtron facility (MAMI).

The expected production process can be described by the isobar model, for example, in the second resonance region $\gamma p \rightarrow N_1^* \rightarrow N_2^* \pi_1^0$ followed by $N_2^* \rightarrow \Delta(1232) \pi_2^0$ where $\Delta(1232)$ decays to $\pi_3^0 p$. The alternative decay branch is $N_2^* \rightarrow f_0(600) p$ where $f_0(600)$ decays to $\pi_2^0 \pi_3^0$. Similar decay chains are expected in the third resonance region, where N_1^* can be one of the sextet N^* states or one of the four Δ^* states mentioned above, but additional decay modes are allowed for the Δ^* states. For example, $\gamma p \rightarrow \Delta^* \rightarrow f_0(600) \Delta(1232)$ followed by $f_0(600) \rightarrow \pi_1^0 \pi_2^0$ and $\Delta(1232) \rightarrow \pi_3^0 p$. Previously the total cross section for the related pion production process, $\pi^- p \rightarrow 3\pi^0 n$, has been used successfully to determine the branching

ratio of $N(1535)_{\frac{1}{2}}^{-} \rightarrow N(1440)_{\frac{1}{2}}^{+} \pi$ [5].

II. EXPERIMENT AND DATA ANALYSIS

The data were collected in 2009 using the upgraded MAMI-C electron microtron that provides a high intensity beam of electrons with maximum energy of 1557 MeV. The MAMI-Glasgow tagging spectrometer [6–8] was used to produce a secondary beam of tagged photons with maximum energy of ≈ 1450 MeV and energy resolution about ± 2 MeV. The Bremsstrahlung beam was incident on a 10-cm-long liquid hydrogen target installed in the center of the Crystal Ball (CB). The spectrometer is a nearly 4π -coverage full absorption spherical calorimeter made of 672 NaI(Tl) triangular-pyramidal crystals arranged in the form of two hemispheres. The crystals are 16 radiation lengths thick and the detector provides a typical energy resolution for photons of $\sigma/E = 1.7\%/[E(\text{GeV})]^{0.4}$. The typical time resolution is 6 ns (FWHM). The detector has two 21° openings, one on the upstream and the other on the downstream side, and a spherical cavity in the center of the sphere allowing installation of the liquid hydrogen target assembly and the particle identification detector (PID) in the middle of the spectrometer. The PID detector surrounding the liquid hydrogen target is made of 24 strips of plastic scintillator 50 cm long and 4 mm thick equipped with a photomultiplier at the upstream end. Although the Crystal Ball is optimized for the detection of photons and electrons, it also has good efficiency for detecting neutrons and protons. See Refs. [9–11] and references therein for a detailed description of the detector.

The geometrical acceptance of the setup was increased by covering the downstream opening in the CB by the TAPS BaF₂ forward wall. In its current configuration, TAPS [12, 13] is comprised of 360 individual barium fluoride (BaF₂) crystals arranged in the form of a hexagonal prism. Each TAPS crystal is shaped as a hexagon with an inscribed diameter of 59 mm and length 250 mm (12 *r.l.*). A time resolution of 160 ps was achieved for the TAPS detector [12]. One crystal in the center of the TAPS detector was removed to allow the beam to exit. The two inner layers of the TAPS BaF₂ crystals (24 crystals in total) were replaced with 72 faster PbWO₄ crystals. However, the PbWO₄ detectors were not used in this analysis. The TAPS assembly is located 147.5 cm downstream of the center of the CB and covers the range in polar angle approximately between 1° and 20° . The combination of CB and TAPS detectors covers $\approx 97\%$ of the solid angle.

The $\gamma p \rightarrow 3\pi^0 p$ events were reconstructed from the pool of six-cluster (six photons only) and seven-cluster (six photons and the proton cluster) events. Both Crystal Ball and TAPS clusters were used in the analysis. A CB cluster consists of the central crystal (the crystal with the maximum deposited energy) and up to 22 surrounding crystals with energies above 1.1 MeV. The energy in the central crystal was required to be above 15 MeV. A TAPS cluster was constructed from the central crystal, which has a minimum energy of 20 MeV, plus up to 18 surrounding crystals with energies 3.5 MeV or higher. The timing information for each crystal was used to ensure that all the hits in a cluster originate from the same particle. The timing coincidence window for the Crystal Ball was set to 70 ns, and for TAPS it was 30 ns. The energy of a photon cluster, calculated as the sum of the energies deposited in all crystals contributing to the cluster, was corrected for the leakage of the electromagnetic shower outside of the cluster boundaries and for nonlinearity of the analog-to-digital converters. The energy-dependent corrections were calculated from a Monte Carlo simulation and verified using the experimental data. For the case of the proton cluster, only the angular information was used.

The detected events were subjected to a fit with kinematical constraints as described in earlier Crystal Ball publications [14, 15]. All 15 combinations of three photon pairs from six-cluster events, and 105 combinations of three pairs plus one proton for seven-cluster events were tested against the $\gamma p \rightarrow 3\pi^0 p \rightarrow 6\gamma p$ hypothesis. The combination with the best χ^2 satisfying the $\gamma p \rightarrow 3\pi^0 p \rightarrow 6\gamma p$ hypothesis at the 95% confidence level (C.L.) was used for further analysis. Therefore the fit was exclusively used to determine the proton cluster and the three pairs of photon clusters from the π^0 decays. The efficiency of the method in respect to the combinatorial background is found to be better than 95%. It was evaluated using Monte Carlo events. An event with n hits in the beam tagger was treated as n independent events with beam energies E_n .

Above $E_\gamma = 709$ MeV the dominant background for $\gamma p \rightarrow 3\pi^0 p$ is the η photoproduction reaction followed by the $\eta \rightarrow 3\pi^0$ decay. In order to handle this background the events were also tested against the $\gamma p \rightarrow \eta p \rightarrow 3\pi^0 p \rightarrow 6\gamma p$ hypothesis. An event was rejected if it satisfied the $\gamma p \rightarrow \eta p \rightarrow 3\pi^0 p \rightarrow 6\gamma p$ hypothesis at the 99% C.L. Figure 1 shows the invariant mass of the reconstructed $3\pi^0$ from the reaction $\gamma p \rightarrow 3\pi^0 p$ integrated over all photon beam energies. The dominant peak in the distribution from $\gamma p \rightarrow \eta p \rightarrow 3\pi^0 p \rightarrow 6\gamma p$ is compared to the Monte Carlo simulation of $\gamma p \rightarrow \eta p \rightarrow 3\pi^0 p \rightarrow 6\gamma p$. The flat distribution under

the peak is due to the direct $\gamma p \rightarrow 3\pi^0 p$ reaction, which is the subject of this paper. The main part of the $\gamma p \rightarrow \eta p \rightarrow 3\pi^0 p$ background was removed using the procedure described above. The residual $\eta \rightarrow 3\pi^0$ background was determined by analyzing the $\gamma p \rightarrow \eta p \rightarrow 3\pi^0 p$ Monte Carlo events as direct $\gamma p \rightarrow 3\pi^0 p$. This part of the background was normalized to the ratio of the reconstructed $\gamma p \rightarrow \eta p \rightarrow 3\pi^0 p$ events in the simulation to the number of $\gamma p \rightarrow \eta p \rightarrow 3\pi^0 p$ detected in the experiment and also subtracted. Additional corrections included subtraction of the good events associated with the accidental hits in the beam tagger ($\sim 13\%$, see Ref. [16] for a detailed description of the procedure) and subtraction of the empty target contribution, which ranges from about 50% close to the threshold to about 3% at higher beam energies. The invariant mass of the directly photoproduced $3\pi^0$ after removal of the $\eta \rightarrow 3\pi^0$ background, the random beam background and the empty target contribution is shown in Fig. 2.

The number of photons in the beam was determined from the number of counts in the photon tagger corrected to the tagger efficiency determined in a series of separate measurements, and to the live time of the data acquisition system; see Ref. [4] for details. In order to verify the absolute normalization of the $\gamma p \rightarrow 3\pi^0 p$ total cross section we have calculated the well-known $\gamma p \rightarrow \eta p$ total cross section. A comparison of our $\sigma_{\text{total}}(\gamma p \rightarrow \eta p)$ to the results obtained in an analysis dedicated to $\gamma p \rightarrow \eta p$ [4] is shown in Fig. 3. Our results are within $\pm 5\%$ agreement with the previously obtained $\gamma p \rightarrow \eta p$ cross sections.

III. RESULTS

The measured $\gamma p \rightarrow 3\pi^0 p$ total cross section is shown in Fig. 4 and listed in Table I. Only statistical uncertainties are shown. The systematical uncertainty is estimated to be 15%. The three main sources of the systematical uncertainty are: (i) the uncertainty in the acceptance calculation associated with complex dynamics of the $\gamma p \rightarrow 3\pi^0 p$ reaction; (ii) the remaining $\gamma p \rightarrow \eta p \rightarrow 3\pi^0 p$ background for $E_\gamma > 710$ MeV; (iii) the background from $\gamma p \rightarrow K_s^0 \Sigma^+$ followed by the decays $K_s^0 \rightarrow 2\pi^0$ and $\Sigma^+ \rightarrow \pi^0 p$. The $\gamma p \rightarrow K_s^0 \Sigma^+$ background contributes at $E_\gamma > 1.05$ GeV and has not been subtracted.

The uncertainty due to the acceptance calculation is estimated to be 5%. The number was obtained from a comparison of $\sigma_{\text{total}}(\gamma p \rightarrow 3\pi^0 p)$ calculated from the integrated number of events to the total cross section obtained by integration of the differential distributions

shown in Fig. 6. The $\gamma p \rightarrow \eta p \rightarrow 3\pi^0 p$ and $\gamma p \rightarrow K_s^0 \Sigma^+$ backgrounds depend strongly on the magnitude of the corresponding total cross sections and therefore vary with the beam energy. However, by our estimate the sum of the two backgrounds is roughly invariant of the beam energy and does not exceed 10% of the number of good $\gamma p \rightarrow 3\pi^0 p$ events.

The total cross section exhibits a smooth behavior from threshold (≈ 492 MeV) to 1.434 GeV where it reaches $2.9 \mu\text{b}$. There is a local maximum of $0.25 \pm 0.01 \mu\text{b}$ at about $E_\gamma = 780$ MeV. This can be compared to the total cross section for η photoproduction at the peak of the $N(1535)\frac{1}{2}^-$ resonance: $\sigma_{\text{total}}(\gamma p \rightarrow \eta p) = 16.0 \pm 0.1 \mu\text{b}$ at $E_\gamma = 780$ MeV [4]. The ratio of these two values is

$$R_\gamma = \frac{\sigma_{\text{total}}(\gamma p \rightarrow 3\pi^0 p)}{\sigma_{\text{total}}(\gamma p \rightarrow \eta p)} = 0.016 \pm 0.001 \quad (1)$$

The corresponding ratio for the pion induced reactions measured in the earlier Crystal Ball experiments [5, 14] is

$$R_\pi = \frac{\sigma_{\text{total}}(\pi^- p \rightarrow 3\pi^0 n)}{\sigma_{\text{total}}(\pi^- p \rightarrow \eta n)} = \frac{0.023 \pm 0.004}{2.63 \pm 0.02} = 0.009 \pm 0.002. \quad (2)$$

The two ratios have very similar values. This can be seen as an indirect confirmation of the earlier estimate $\mathcal{B}(S_{11}(1535) \rightarrow P_{11}(1440)\pi) \approx 0.08$ [5]. The slight difference between the two ratios can possibly be attributed to the different interference between $N(1520)\frac{3}{2}^-$ and $N(1535)\frac{1}{2}^-$ and to the difference in the non-resonant background in photo- and pion production.

The isospin-conjugated 3π photoproduction processes were measured previously at higher beam energies in several bubble chamber experiments [17, 18]. In particular, the $\gamma p \rightarrow \pi^+ \pi^- \pi^0 p$ total cross section grows rapidly to about $20 \mu\text{b}$ from threshold to $E_\gamma = 2$ GeV and then declines gradually to about $10 \mu\text{b}$ at $E_\gamma = 6$ GeV forming a broad peak with a maximum at around 2 GeV. Assuming similar behavior for the $\gamma p \rightarrow 3\pi^0 p$ cross section we can speculate that the rapid growth of the $3\pi^0$ cross section from threshold to 1.4 GeV is determined by the contributions from N^* and Δ^* with masses 1.9–2.2 GeV/ c^2 .

In order to study in more detail the enhancements at $\sqrt{s} \approx 1.5$ GeV and 1.7 GeV we have fitted the cross section with a third-degree polynomial excluding the enhanced areas from the fit. The result of the fit is shown in Fig. 4 by the dashed line. The part of the distribution above the fit curve is shown in Fig. 5. A Breit-Wigner fit of the two peaks in Fig. 5 gives the positions of the peaks $\sqrt{s} = 1.54$ GeV and 1.73 GeV and the widths $\Gamma = 43$ MeV

and 83 MeV, respectively. The enhancements can possibly be attributed to the interference between the excited states in the second and the third resonance regions, although the structure at $\sqrt{s} = 1.54$ GeV can be partially due to the remaining $\gamma p \rightarrow \eta p$ background. It is worth noting that the $\gamma p \rightarrow \pi^0 \pi^0 p$ total cross section exhibits two similar enhancements with masses 50-70 MeV lower than the ones observed in our experiment [19]. Figure 6 shows the differential cross section for the angular distribution of the recoil proton in $\gamma p \rightarrow 3\pi^0 p$ in the center-of-mass frame for four beam energy intervals. The distributions all show a quite strong angular dependence. We fitted the angular distributions with expansions in terms of Legendre polynomials. Figure 7 shows the dependence of the Legendre coefficients $A_1 - A_4$ on the beam energy. The distributions of all coefficients show substantial structure.

Further information on the dynamics of the $3\pi^0$ photoproduction can be extracted from the Dalitz plot distributions. Examples of such distributions are shown in Fig. 8. The axes of the Dalitz plot are $M^2(\pi^0 p)$ and $M^2(\pi^0 \pi^0)$. Each event has three entries on the distribution representing three different combinations of $\pi^0 p$ and $\pi^0 \pi^0$.

The Dalitz plot reflects the complex dynamics of the reaction. We expect that the $\pi^0 p$ interactions lead to $\Delta(1232)$ formation, which shows up in Fig. 9 as a strong peak near $1.5 \text{ GeV}^2/c^4$. The $\Delta(1232)$ contribution is also seen in the ratio of the $M^2(\pi^0 p)$ projection of the Dalitz plot obtained from the data to the results of the Monte Carlo simulation generated according to phase-space distribution. The ratios are shown in Fig. 11 for four beam intervals. The contribution from the $\Delta(1232)$ is also seen at around $1.5 \text{ GeV}^2/c^4$. The mass of the Δ peak on the projection is slightly off. This is a combinatorial effect due to the fact that all three combinations of $M^2(\pi^0 p)$ are plotted.

The $\pi^0 \pi^0$ interaction leads to the intermediate $f_0(600)$ resonance. Its mass is not well known. The projections of the Dalitz plot to $M^2(\pi^0 \pi^0)$ axis do not show any substantial structures in comparison to the phase-space distribution, see Fig. 10. These features have been seen in the reaction $\pi^- p \rightarrow \pi^0 \pi^0 n$ [20] as well. No substantial contribution from $f_0(600) \rightarrow 2\pi^0$ was observed.

To summarize our results, the total cross section for $\gamma p \rightarrow 3\pi^0 p$ has been measured for the first time from threshold to 1.4 GeV. The excitation function for $\sigma_{\text{total}}(\gamma p \rightarrow 3\pi^0 p)$ has two broad enhancements at $\sqrt{s} \approx 1.5$ GeV and 1.7 GeV. The ratio $\sigma_{\text{total}}(\gamma p \rightarrow 3\pi^0 p)/\sigma_{\text{total}}(\gamma p \rightarrow \eta p) = 0.014 \pm 0.001$ was obtained at $\sqrt{s} \approx 1.5$ GeV confirming previous results for $\mathcal{B}(S_{11}(1535) \rightarrow P_{11}(1440)\pi)$.

IV. ACKNOWLEDGMENTS

The success of the experiment on the $3\pi^0$ photoproduction has been made possible by the use of the Crystal Ball neutral meson spectrometer with its 97% acceptance per photon. We thank SLAC for letting us use the Crystal Ball. The authors very much appreciate the dedicated work of the MAMI accelerator group. We also thank the undergraduate students of Mount Allison University and the George Washington University for their assistance in data taking. This work was supported by DOE and NSF of the U.S., EPSRC and STFC of the U.K., NSERC of Canada, the Deutsche Forschungsgemeinschaft (SFB 443) of Germany, and DFG-RFBR (Grant No.09-02-91330) of Germany and Russia, SNF of Switzerland and the European Community-Research Infrastructure Activity under the FP6 “Structuring the European Research Area” program (Hadron Physics, contract number RII3-CT-2004-506078).

-
- [1] L. Y. Glozman, Phys. Lett. B **475**, 329 (2000).
 - [2] L. Y. Glozman and A. V. Nefediev, Nucl. Phys. A **807**, 38 (2008).
 - [3] R. A. Arndt, W. J. Briscoe, I. I. Strakovsky, and R. L. Workman, Phys. Rev. C **74**, 045205 (2006).
 - [4] E. F. McNicoll et al., Phys. Rev. C **82**, 035208 (2010).
 - [5] A. Starostin et al., Phys. Rev. C **67**, 068201 (2003).
 - [6] I. Anthony et al., Nucl. Instr. Meth. A **301**, 230 (1991).
 - [7] S. J. Hall et al., Nucl. Instr. Meth. A **368**, 698 (1996).
 - [8] J. C. McGeorge et al., Eur. Phys. J. A **37**, 129 (2008).
 - [9] A. Starostin et al., Phys. Rev. C **64**, 055205 (2001).
 - [10] S. Prakhov et al., Phys. Rev. C **78**, 015206 (2008).
 - [11] C. M. Tarbert et al., Phys. Rev. Lett. **100**, 132301 (2008).
 - [12] R. Novotny, IEEE Trans. Nucl. Sci. **38**, 379 (1991).
 - [13] R. Gabler et al., Nucl. Instr. Meth. A **346**, 168 (1994).
 - [14] S. Prakhov et al., Phys. Rev. C **72**, 015203 (2005).
 - [15] V. Blobel, documentation and source are available at <http://www.desy.de/~blobel/>.
 - [16] S. Schumann et al., Eur. Phys. J. A **43**, 269 (2010).

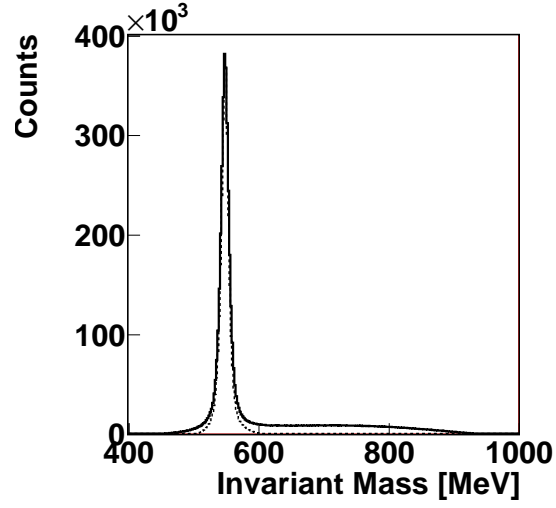


FIG. 1: Invariant mass spectrum of $3\pi^0$ measured in the reaction $\gamma p \rightarrow 3\pi^0 p \rightarrow 6\gamma p$ and integrated over the photon beam energy range from threshold to 1.43 GeV. The dominant peak is due to $\gamma p \rightarrow \eta p \rightarrow 3\pi^0 p$ and the smooth background under the peak comes from the $\gamma p \rightarrow 3\pi^0 p$ direct production. The width of the η peak has $\sigma = 6.9$ MeV. The peak is compared to the results of the Monte Carlo simulation shown by the dashed line.

- [17] W. Struczinski et al., Nucl. Phys. **B108**, 45 (1976).
- [18] H. H. Bingham et al., Phys. Rev. D **8**, 1277 (1973).
- [19] U. Thoma et al., Phys. Lett. **B659**, 87 (2008).
- [20] S. Prakhov et al., Phys. Rev. C **69**, 045202 (2004).

TABLE I: $\gamma p \rightarrow 3\pi^0 p$ total cross section. Only statistical uncertainties are listed.

$E_\gamma(\text{MeV}/c)$	$\sigma_{\text{total}}(\gamma p \rightarrow 3\pi^0 p)(\mu\text{b})$	$E_\gamma(\text{MeV}/c)$	$\sigma_{\text{total}}(\gamma p \rightarrow 3\pi^0 p)(\mu\text{b})$
520 ± 9	<0.02	1044 ± 8	0.841 ± 0.012
538 ± 9	<0.02	1059 ± 8	0.905 ± 0.014
555 ± 9	<0.02	1074 ± 8	1.012 ± 0.015
573 ± 9	0.002 ± 0.001	1089 ± 7	1.099 ± 0.013
591 ± 9	0.002 ± 0.001	1104 ± 7	1.147 ± 0.013
608 ± 9	0.003 ± 0.001	1118 ± 7	1.236 ± 0.015
626 ± 9	0.005 ± 0.001	1133 ± 7	1.315 ± 0.015
643 ± 9	0.009 ± 0.002	1147 ± 7	1.389 ± 0.018
661 ± 9	0.014 ± 0.002	1161 ± 7	1.405 ± 0.015
678 ± 9	0.027 ± 0.002	1175 ± 7	1.452 ± 0.016
696 ± 9	0.035 ± 0.003	1189 ± 7	1.510 ± 0.017
713 ± 9	0.058 ± 0.005	1202 ± 7	1.527 ± 0.017
730 ± 9	0.074 ± 0.013	1216 ± 7	1.599 ± 0.018
748 ± 9	0.125 ± 0.007	1229 ± 7	1.638 ± 0.018
765 ± 9	0.178 ± 0.009	1242 ± 6	1.769 ± 0.027
782 ± 9	0.243 ± 0.009	1255 ± 6	1.808 ± 0.019
799 ± 9	0.256 ± 0.011	1267 ± 6	1.862 ± 0.029
816 ± 8	0.263 ± 0.010	1280 ± 6	1.933 ± 0.021
833 ± 8	0.286 ± 0.012	1292 ± 6	1.940 ± 0.029
850 ± 8	0.297 ± 0.015	1304 ± 6	2.121 ± 0.022
867 ± 8	0.300 ± 0.012	1316 ± 6	2.141 ± 0.023
884 ± 8	0.335 ± 0.019	1328 ± 6	2.203 ± 0.027
900 ± 8	0.362 ± 0.011	1339 ± 6	2.372 ± 0.028
917 ± 8	0.376 ± 0.010	1350 ± 6	2.379 ± 0.030
933 ± 8	0.413 ± 0.010	1362 ± 6	2.552 ± 0.037
949 ± 8	0.459 ± 0.010	1374 ± 6	2.574 ± 0.026
965 ± 8	0.498 ± 0.010	1386 ± 6	2.657 ± 0.029
981 ± 8	0.539 ± 0.014	1399 ± 6	2.765 ± 0.027
997 ± 8	0.607 ± 0.010	1412 ± 6	2.900 ± 0.030
1013 ± 8	0.672 ± 0.010	1424 ± 6	3.045 ± 0.035
1028 ± 8	0.763 ± 0.011	1434 ± 5	3.034 ± 0.041

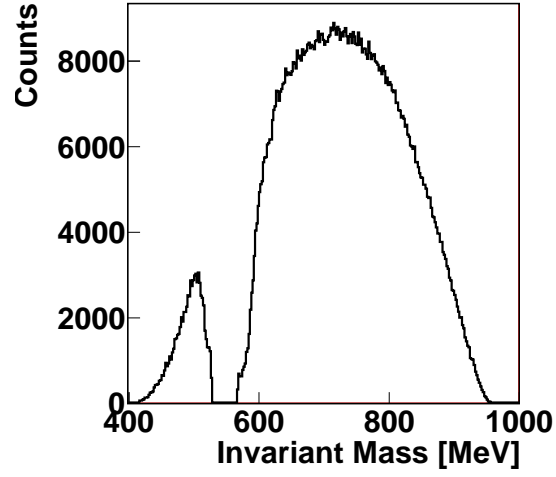


FIG. 2: Invariant mass spectrum of $3\pi^0$ from $\gamma p \rightarrow 3\pi^0 p \rightarrow 6\gamma p$ after subtraction of the $\gamma p \rightarrow \eta p \rightarrow 3\pi^0 p$ background and other backgrounds; see text for details.

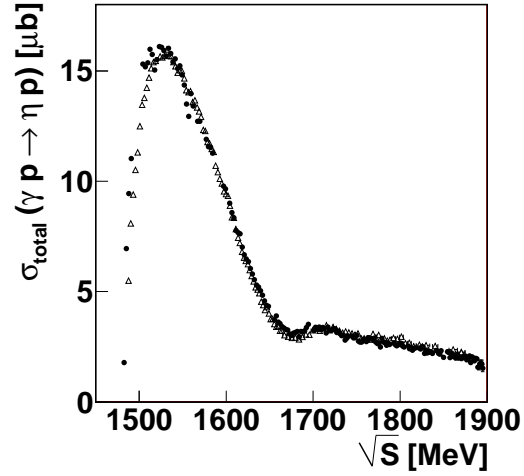


FIG. 3: The $\gamma p \rightarrow \eta p$ total cross section determined in this work (black dots) compared to the results from Ref. [4] (open triangles).

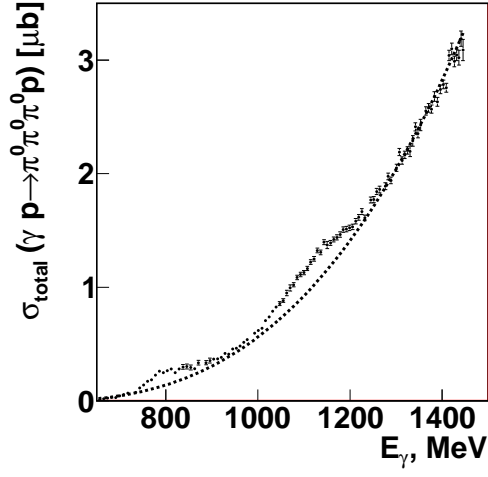


FIG. 4: The $\gamma p \rightarrow 3\pi^0 p$ total cross section obtained in our experiment. The dotted line indicates a polynomial fit to the experimental data; see text for details.

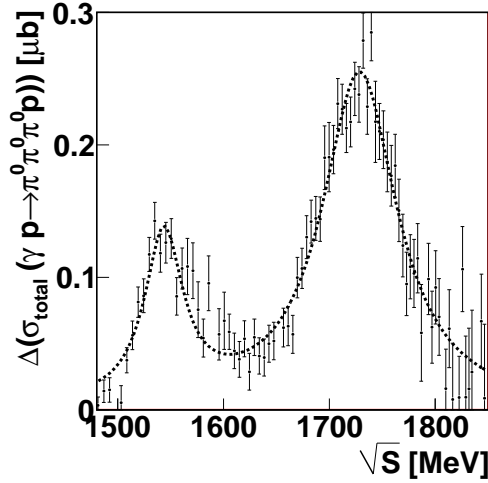


FIG. 5: The difference between the $\gamma p \rightarrow 3\pi^0 p$ total cross section and the result of the polynomial fit shown on the previous figure. The dotted line shows the fit of the difference with two Breit-Wigner distributions. The peak positions from the fit are 1.53 GeV and 1.74 GeV.

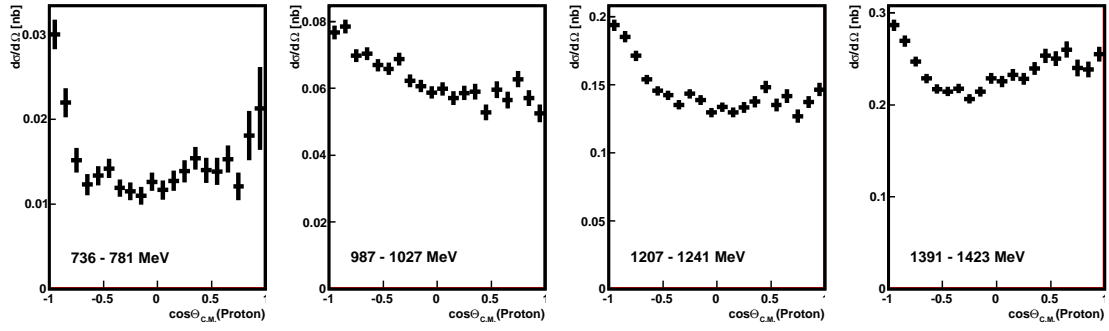


FIG. 6: Differential cross sections $d\sigma/d\Omega$ for the Θ_p in the center-of-mass frame for four beam energy intervals.

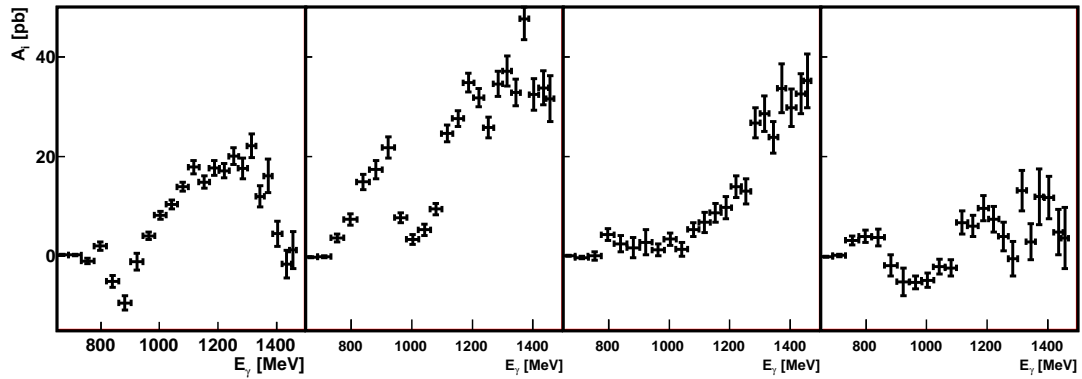


FIG. 7: Legendre coefficients $A_1 - A_4$ (from left to right) from the fit to $d\sigma/d\Omega$ for the Θ_p differential cross section.

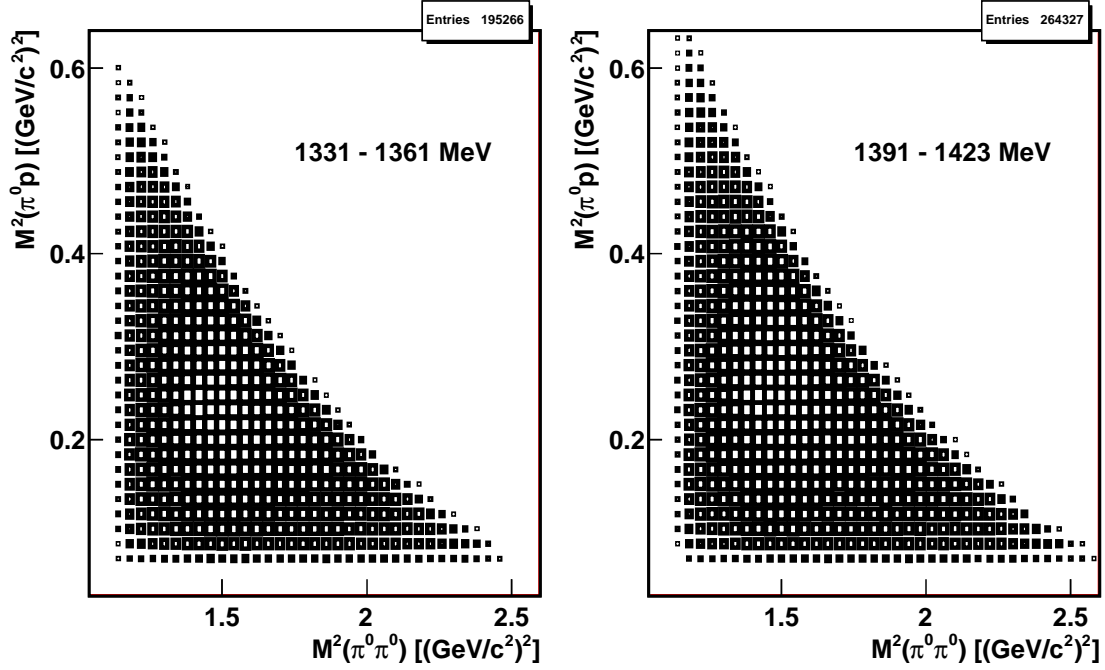


FIG. 8: Examples of the $\gamma p \rightarrow 3\pi^0 p$ Dalitz plots. The x -axis shows $M^2(\pi^0 p)$ and the y -axis $M^2(\pi^0 \pi^0)$. Each events has three entries in the distribution representing different $\pi^0 p$ and $\pi^0 \pi^0$ combinations.

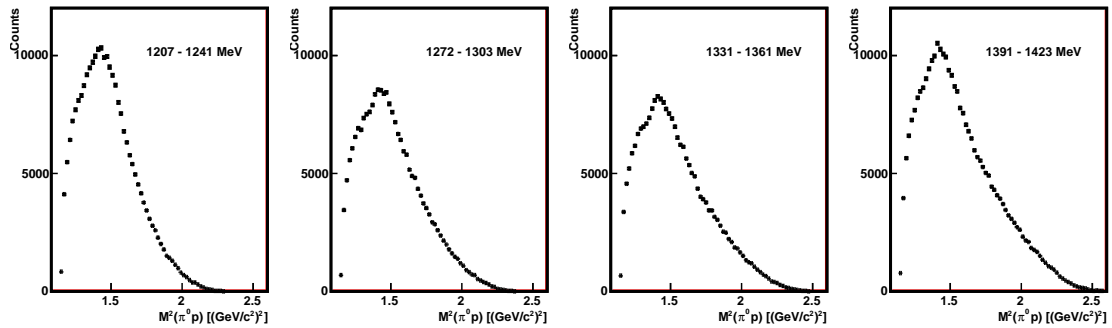


FIG. 9: Projection of the Dalitz plot onto the $M^2(\pi^0 p)$ axis for four beam energy intervals.

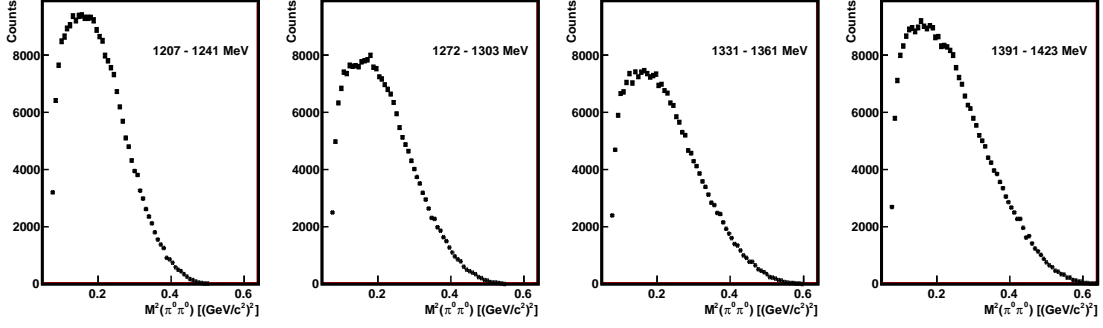


FIG. 10: Projection of the $\gamma p \rightarrow 3\pi^0 p$ Dalitz plot unto the $M^2(\pi^0\pi^0)$ axis for four beam energy intervals.

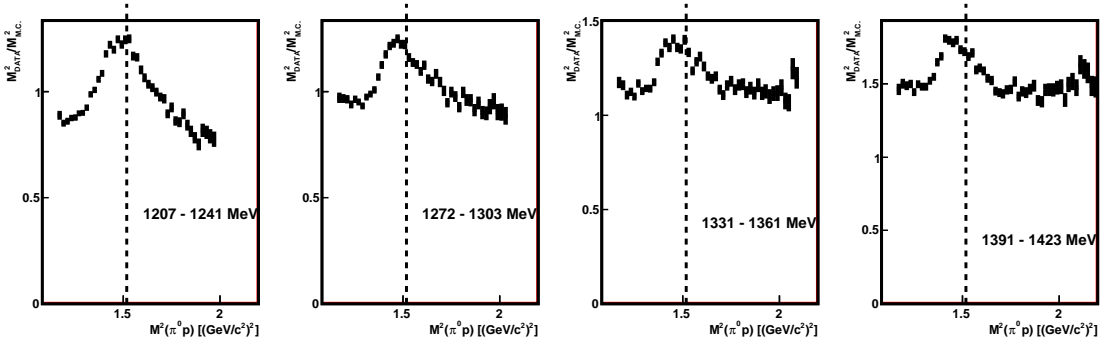


FIG. 11: Ratio of the $M^2(\pi^0 p)$ projections of the Dalitz plot obtained from the experimental data to the simulated distribution generated according to phase-space. The dashed line on the plots indicates the $\Delta(1232)$.